Textural and Mineralogical Analysis of Volcanic Rocks by µ-XRF Mapping

Textural and mineralogical analysis of volcanic rocks by µ-XRF mapping

Running head: Petrographic analysis by µ-XRF mapping

Luigi Germinario[a,*], Roberto Cossio[b], Lara Maritan[a], Alessandro Borghi[b], Claudio Mazzoli[a]

[a] Dipartimento di Geoscienze, Università degli Studi di Padova, Via Gradenigo 6, 35131 Padova, Italy

[b] Dipartimento di Scienze della Terra, Università degli Studi di Torino, Via Valperga Caluso 35, 10125 Torino, Italy

* Corresponding author. Email address: luigi.germinario@gmail.com Phone: +393483164080

Abstract

In this study, µ-XRF was applied as a novel surface technique for quick acquisition of elemental X-ray maps of rocks, image analysis of which provides quantitative information on texture and rock-forming minerals. Bench-top µ-XRF is cost-effective, fast and non-destructive, can be applied to both large (up to a few tens of cm) and fragile samples, and yields major and trace element analysis with good sensitivity. Here, X-ray mapping was performed with a resolution of 103.5 µm and spot size of 30 µm over areas of about 5 x 4 cm of samples of Euganean trachyte, a volcanic porphyritic rock from the Euganean Hills (NE Italy), traditionally used in cultural heritage. The relative abundance of phenocrysts and groundmass, as well as the size and shape of the various mineral phases, were obtained from image analysis of the elemental maps. The quantified petrographic features allowed identifying various extraction sites, revealing an objective method for archaeometric provenance studies exploiting µ-XRF imaging.

Keywords

Micro-XRF imaging; X-ray maps; Quantitative texture analysis; Modal composition; Euganean trachyte; Provenance study.

1. Introduction

The texture of a rock represents the geometric complexity of its constituents, i.e., crystals, grains, glass and pores, as defined by their size, shape, position, orientation and mutual spatial relationships. The description and quantification of texture is a key topic in petrology, as it provides information about petrogenetic processes and supports the development of physical models, texture being influenced by the growth rate, dissolution, movement and deformation of minerals during rock formation (Higgins, 2006; Jerram and Kent, 2006). Textural characteristics are also studied in a number of related disciplines, e.g., in archaeometry for information on how stone can resist deterioration (Steiger et al., 2014), or in engineering for inferring the quality of stone materials (Přikryl, 2006; Ozturk and Nasuf, 2013).

From a geometric viewpoint, texture is a three-dimensional property, so that its quantification by two-dimensional methods is indirect and requires extrapolation of data (Higgins, 2000). Nevertheless, 2D methods are still frequently preferred, as sample and grain size is not strongly constrained, the necessary equipment is less expensive, and the analyses are non-destructive or micro-destructive (Jerram and Higgins, 2007; Baker et al., 2012). Modern 2D methods rely on the extraction of textural information after automated analysis of digital images, acquired on a plane rock-sample surface with optical or electronic techniques. The former provides very cost-effective transmitted-light photos taken on thin sections with a polarising microscope or image scanner, but resolution is often poor and, in most cases, image processing is slow and complex for rocks composed of many phases and crystals (Tarquini and Armienti, 2003; Tarquini and Favalli, 2010). Segmentation may be difficult when different mineral phases with similar colours (under parallel polars) and interference colours (under crossed polars) are present in the same sample: in these cases, automatic attribution to a specific mineral phase is impossible, and assisted recognition is required to produce accurate data. Conversely, electronic techniques are based on scanning electron microscopy (SEM) or electron probe microanalysis (EPMA) to generate X-ray maps: chemical information is directly available and image analysis is fast, but acquisition may be extremely time-

consuming, so it is usually applied only on millimetric or sub-millimetric surfaces. Back-scattered electron images may also be used, but phases with similar mean atomic numbers cannot easily be discriminated (Lindqvist and Åkesson, 2001; Higgins, 2006). Therefore, if mineralogy is a concern, X-ray maps are the most useful source of information, as they can also indirectly provide information on the modal composition of rocks, much more quickly than manual point counting under the microscope (Maloy and Treiman, 2007).

Recent progress in X-ray optics has produced compact spectrometers for micro X-ray fluorescence (μ-XRF), once the prerogative of only a few synchrotron-based systems (Behrends and Kleingeld, 2009; Mera et al., 2015). μ-XRF works on the same principles as standard XRF, but high-intensity, finely collimated X-ray beams are used. In bench-top instruments, the beam can reach a spot size of 10 μm and is usually generated by a polycapillary lens, a compact device composed of a bundle of curved, micrometric glass channels, through which photons are focused by multiple internal reflections. The secondary X-rays emitted by the sample are detected in energy-dispersion mode from discrete points, lines or areas, providing elemental maps. Detection limits are between 10 and 100 ppm for transition elements, and typically every element from Na (Z = 11) to U (Z = 92) can be measured (Janssens, 2004; Behrends and Kleingeld, 2009; Haschke et al., 2012; Vaggelli and Cossio, 2012). The resolution achievable with μ-XRF is much lower than that of SEM or EPMA, but the advantages outweigh this disadvantage: the instrument is less expensive, analyses are faster, can be performed in both air and under vacuum, and are not affected by electronic charging effects (Higgins, 2006); large objects (up to a few tens of cm) can be analysed and, although flat surfaces produce better results, no sample preparation is required. In addition, the latest advances in μ-XRF technology have led to the development of portable instruments and confocal spectrometers for 3D analysis (Malzer and Kanngießer, 2005; Kanngießer et al., 2012). For all these reasons, μ-XRF is increasingly applied in archaeometric studies, in which non-invasive and non-destructive techniques are needed to analyse artistic and archaeological materials (Janssens et al., 2000; Rindby and Janssens, 2002; Mantouvalou et al., 2011; Vaggelli et al., 2013; Angelici et al., 2015).

In this paper, μ-XRF mapping coupled with image analysis was tested for rapid acquisition of quantitative textural and mineralogical information on volcanic porphyritic rocks. The material analysed was Euganean trachyte, quarried in the district of the Euganean Hills (Veneto, NE Italy) and widely used in cultural heritage. The possibility of applying μ-XRF imaging to archaeometric studies, with quantitative petrographic criteria to identify and discriminate quarry provenance, was also verified.

2. Materials

Euganean trachyte is a subvolcanic porphyritic rock that formed during the intermediate and acidic activity in the lower Oligocene in the area of the Euganean Hills (De Vecchi et al., 1976; Milani et al., 1999). This volcanic complex is the most important district in Italy for trachyte, which has been extensively quarried in more than 70 open pits, probably since the 7th century BC and still ongoing on a small scale. Historically, this activity has influenced the landscape and local economy but, above all, it represents the starting point of the widespread use of trachyte in the cultural heritage of northern and central Italy. In fact, from Roman times onwards, Euganean trachyte has been extensively used as a building material in many monuments and infrastructures, as well as in common constructions and artefacts, thanks to its durability and excellent technical properties (Cattani et al., 1997; Renzulli et al., 1999, 2002a, 2002b; Capedri et al., 2000, 2003; Capedri and Venturelli, 2003, 2005; Santi and Renzulli, 2006; Antonelli and Lazzarini, 2010, 2012; Maritan et al., 2013).

In this paper, 14 trachyte samples were analysed, collected from nine quarries in Monselice, Monte Merlo and Monte Oliveto, the localities representing the main historical quarry sites in the Euganean district (Previato et al., 2014). These representative samples are a subset selected among 24 specimens collected in the above mentioned localities, after a detailed analysis by optical microscopy and SEM, which examined both textural and mineralogical variability within the same quarry and magmatic body. The results of preliminary petrographic characterisation of the samples,

carried out on separate thin sections under a polarising microscope, are shown in Table 1 and Fig. 1. Attribution to the correct mineral phase was also confirmed by EPMA analyses, performed on all thin sections.

3. Methods

The samples were prepared in the form of 7 x 7 x 1 cm tiles and mapped on a smooth flat surface with an EDAX Eagle III XPL bench-top spectrometer, equipped as follows: X-ray tube with Rh anode; polycapillary lens for beam focusing on spots of 30 to 300 µm; Si(Li) energy-dispersive detector with Be window; large sample chamber, operating in air or under vacuum; motorised x-y-z sample staging; two cameras for sample viewing. The instrument and data were controlled by EDAX Vision 32 software. During map acquisition, a spot size of 30 µm and a resolution (step size) of 103.5 µm were used to analyse a 512 x 400 pixel grid, i.e., a total area of about 5 x 4 cm. The X-ray tube was operated at 40 kV and 1 mA, and a time constant of 2.5 µs and a dwell time of 200 ms were chosen. Count maps of the following elements were recorded: Na, Mg, Al, Si, P, S, K, Ca, Ti, Fe, Sr, Zr, Ba. Overall analytical time was about 18 hours for each automated overnight run. The Na maps proved to have a low signal/noise ratio. This problem could have been avoided with higher resolution or increased dwell time, but would have led to far longer analytical times.

The resulting maps (Fig. 2) were processed by digital image analysis with open-source software packages (ImageJ v1.48 and MultiSpec v3.4), in order to extract the relative abundances of the rock constituents, i.e., phenocrysts and groundmass, and the textural features of the various mineral phases. A pre-processing step of contrast/brightness adjustment and noise reduction preceded for each elemental map. The most significant maps from each sample were then superimposed and analysed as multispectral images, in which the various mineral phases were identified by their chemical composition and segmented according to manually defined training pixels. Lastly, classified images were obtained, after ECHO spectral/spatial classification with Fisher's linear discriminant algorithm; the classified images were subjected to colour thresholding and, for each

colour-assigned constituent and phase, particle analysis was also performed. Quantitative textural and mineralogical data were extracted through calculation of the following descriptors of size and shape of each discrete grain: area, perimeter, Feret diameter, circularity and aspect ratio (the Feret diameter is the longest distance between any two points along the selected particle boundary, i.e., the maximum dimension of a grain; circularity is calculated as $4\pi \cdot \text{area}/\text{perimeter}^2$: a value of 1 indicates a perfect circle, values approaching 0 denote an increasingly elongated shape; aspect ratio AR = Feret diameter/minimum Feret diameter: the ratio between the major and minor axes of an ellipse fitted to the selected particle boundary, thus expressing the average degree of elongation of that grain). It should be noted that a discrete grain, separated from the surrounding groundmass, is defined here according to the values of spot size and resolution chosen for the analyses. Lastly, petrographic parameters were statically processed by Principal Component Analysis (PCA) with the Statgraphics Centurion XVI software package.

4. Results and discussion

With the present experimental setup, data on crystals mostly above ~100 μm are given, which comprise, for each sample, the totality of phenocrysts (here defined as crystals distinctly larger – at least 5 times – than the grains of the groundmass). The smallest grain size measured was typically affected by the used resolution, but also by variable factors, such as orientation and shape of crystals and their spatial relationships with the position of mapping points and the chosen spot size.

Comparisons among representative classified images for each quarry locality (Fig. 3) clearly showed that trachytes from the various areas differ in terms of type, absolute and relative abundance and grain size of the phenocrysts, as well as the percentage of groundmass. This was confirmed by the porphyritic index (total percentage of phenocrysts) and the abundance of the various phases for each sample (Table 2).

Although a certain variability occurs in each quarry locality, trachytes from Monselice and Monte Merlo had a higher phenocryst-groundmass ratio than those from Monte Oliveto. Another main

difference was feldspar content, although mafic and accessory minerals had random distribution. The trachyte from Monselice and Monte Merlo contained a higher feldspar fraction (total content) than that from Monte Oliveto, where this content was always lower than 22%. In addition, plagioclase was not found in Monselice, although it does occur in the other two localities, the highest average concentration being in Monte Merlo (5.60%). Sanidine was found in almost all samples, although only in negligible amounts (less than 1%), except for the samples from Monselice and in two samples from Monte Merlo (MRL-03) and Monte Oliveto (OLV-12). PCA, measuring the percentages of the various mineral phases in the phenocrysts and the percentage of groundmass in each sample (Fig. 4a), showed that trachyte from the three localities can be discriminated on the basis of these parameters. According to the Mahalanobis distance, 100% of samples were correctly classified *a priori*, and none was assigned to a different group by the classification routine of discriminant analysis.

When the crystal-size distribution of feldspars was examined (Table 3, Fig. 5), the Monselice trachyte turned out to contain the largest feldspars, with a maximum area of about 40 mm^2 and maximum Feret diameter of about 10 mm, with grain size scattered over a rather broad but uneven range. The Monte Oliveto trachyte was characterised by fine-grained feldspars, mainly under 5 mm^2 and never exceeding 14 mm^2, and a Feret diameter mostly below 2 mm. The Monte Merlo trachyte showed intermediate characteristics, feldspars displaying seriate distribution from coarse- to fine-grained phenocrysts. PCA of the crystal-size distribution of the whole feldspar fraction, separating the concentrations of anorthoclase, plagioclase and sanidine (Fig. 5b), shows that trachytes from the three localities cluster according to the following parameters: high concentration of anorthoclase and coarser feldspars at Monselice; high content of fine-sized feldspars at Monte Oliveto; high plagioclase and intermediate-sized feldspars at Monte Merlo. Also in this case, discriminant analysis confirmed that the samples were correctly classified *a priori*, and none was assigned to a different group by the classification routine.

Although grain-size properties proved to be efficient in discriminating the various quarrying localities, crystal shape turned out to be unsuitable for this purpose.

The textural and mineralogical quantitative information obtained from image analysis of the μ-XRF maps matched the previous qualitative observations under the microscope, but had greater statistical representativeness, since they were taken on areas twice as large as standard thin sections. In this sense, although preliminary petrographic characterisation may aid the processing of X-ray maps, it is not strictly necessary, provided that an approximate evaluation is made about the detectable mineral phases.

The petrographic differences observed among the trachytes subjected to μ-XRF suggested that the results could be applied to archaeometry, with the aim of proposing new parameters for identifying and discriminating the quarry of provenance for Euganean trachyte. Knowing exactly where the stone used in archaeological or historical objects was quarried provides clues about ancient trades, circulation of raw and finished stone materials and artefacts, quarry work and sources of stone supply. It can also aid reconstruction of the territorial organisation of settlements and, lastly, can provide useful indications about the most suitable materials for restoration. The Euganean trachytic rocks are very similar in both bulk chemical composition and macroscopic and microscopic characteristics. This is why the most traditional methods used in provenance studies, such as XRF analyses or thin-section observations, are not sufficient to differentiate the rocks from various outcrops and quarrying localities. Recent studies do demonstrate that the discrimination criteria generally accepted in the literature are partially unreliable (Maritan et al., 2013). The problem is further complicated by the widespread use of trachyte and the existence of many ancient quarries in the Euganean Hills. In this regard, PCA on both textural and mineralogical data extracted by μ-XRF imaging aimed at verifying the validity of the discriminating parameters inferred from the raw results.

5. Conclusions

Complete petrographic characterisation of samples of Euganean trachyte, obtained from image analysis of X-ray maps, clearly shows the advantages of bench-top μ-XRF mapping as a non-destructive technique for textural and mineralogical quantitative analysis of porphyritic rocks, provided that their grain size matches the resolution limits of the spectrometer used. Given this, if modal analysis is the only concern, μ-XRF can also be extended to rocks with equigranular textures and with multiple minerals of the same phase in mutual contact.

Although it does not introduce really new analytical possibilities, the potential of μ-XRF mapping for imaging – more than for spot analyses, for which it has mostly been used so far – are promising, and are enhanced by cost-effective instrumentation, low detection limits, short analysis times, and the possibility of analysing large fragile objects. Thanks to these characteristics, μ-XRF exceeds the possibilities of SEM and EPMA, which can still serve as preparatory techniques when higher resolution, sensitivity or accuracy are required.

The suggestion of applying μ-XRF to archaeometric provenance studies is only one of its potential uses. However, the quality of the results from the main historical quarries of Euganean trachyte encourages extending this type of research to the entire Euganean district, in order to create a complete reference database. This is a novel alternative approach to classic provenance studies of stone, traditionally performed according to chemical or microchemical properties, without taking texture into account.

Acknowledgements

This work was funded by the Universities of Padova and Torino, with Institutional Research Funds. The authors are also very grateful to G. Walton, who revised the English text.

References

ANGELICI, D., BORGHI, A., CHIARELLI, F., COSSIO, R., GARIANI, G., LO GIUDICE, A., RE, A., PRATESI, G. & VAGGELLI, G. (2015). μ-XRF analysis of trace elements in lapis lazuli-forming minerals for a provenance study. *Microscopy and Microanalysis* **21**, 526–533.

ANTONELLI, F. & LAZZARINI, L. (2010). Mediterranean trade of the most widespread Roman volcanic millstones from Italy and petrochemical markers of their raw materials. *Journal of Archaeological Science* **37**, 2081–2092.

ANTONELLI, F. & LAZZARINI, L. (2012). The first archaeometric characterization of Roman millstones found in the Aquileia archaeological site (Udine, Italy). *Archaeometry* **54** (1), 1–17.

BAKER, D.R., MANCINI, L., POLACCI, M., HIGGINS, M.D., GUALDA, G.A.R., HILL, R.J. & RIVERS, M.L. (2012). An introduction to the application of X-ray microtomography to the three-dimensional study of igneous rocks. *Lithos* **148**, 262–276.

BEHRENDS, T. & KLEINGELD, P. (2009). Bench-top micro-XRF - a useful apparatus for geochemists? *Geochemical News* **138**, 1–5.

CAPEDRI, S., GRANDI, R. & VENTURELLI, G. (2003). Trachytes used for paving Roman roads in the Po Plain: characterization by petrographic and chemical parameters and provenance of flagstones. *Journal of Archaeological Science* **30**, 491–509.

CAPEDRI, S. & VENTURELLI, G. (2003). Trachytes employed for funerary artefacts in the Roman Colonies Regium Lepidi (Reggio Emilia) and Mutina (Modena) (Italy): provenance inferred by petrographic and chemical parameters and by magnetic susceptibility. *Journal of Cultural Heritage* **4**, 319–328.

CAPEDRI, S. & VENTURELLI, G. (2005). Provenance determination of trachytic lavas, employed as blocks in the Romanesque cathedral of Modena (Northern Italy), using magnetic susceptibility, and petrographic and chemical parameters. *Journal of Cultural Heritage* **6**, 7–19.

CAPEDRI, S., VENTURELLI, G. & GRANDI, R. (2000). Euganean trachytes: discrimination of quarried sites by petrographic and chemical parameters and by magnetic susceptibility and its bearing on the provenance of stones of ancient artefacts. *Journal of Cultural Heritage* **1**, 341–364.

CATTANI, M., LAZZARINI, L. & FALCONE, R. (1997). Macine protostoriche dall'Emilia e dal Veneto: note archeologiche, caratterizzazione chimico-petrografica e determinazione della provenienza. *Padusa* **31**, 105–137.

DE VECCHI, G.P., GREGNANIN, A. & PICCIRILLO, E.M. (1976). Tertiary volcanism in the Veneto: magmatology, petrogenesis and geodynamic implications. *Geologische Rundschau* **65**, 701–710.

HASCHKE, M., ROSSEK, U., TAGLE, R. & WALDSCHLÄGER, U. (2012). Fast elemental mapping with micro-XRF. *Advances in X-ray Analysis* **55**, 286–298.

HIGGINS, M.D. (2000). Measurement of crystal size distributions. *American Mineralogist* **85**, 1105–1116.

HIGGINS, M.D. (2006). *Quantitative textural measurements in igneous and metamorphic petrology*. New York: Cambridge University Press.

JANSSENS, K. (2004). X-ray based methods of analysis. In *Non-destructive microanalysis of cultural heritage materials*, Janssens, K. & Van Grieken, R. (Eds.), pp. 129–226. Comprehensive Analytical Chemistry, Vol. XLII. Amsterdam: Elsevier.

JANSSENS, K., VITTIGLIO, G., DERAEDT, I., AERTS, A., VEKEMANS, B., VINCZE, L., WEI, F., DERYCK, I., SCHALM, O., ADAMS, F., RINDBY, A., KNÖCHEL, A., SIMIONOVICI, A. & SNIGIREV, A. (2000). Use of microscopic XRF for non-destructive analysis in art and archaeometry. *X-Ray Spectrometry* **29**, 73–91.

JERRAM, D.A. & HIGGINS, M.D. (2007). 3D analysis of rock textures: quantifying igneous microstructures. *Elements* **3**, 239–245.

JERRAM, D.A. & KENT, A.J.R. (2006). An overview of modern trends in petrography: textural and microanalysis of igneous rocks. *Journal of Volcanology and Geothermal Research* **154**, 7–9.

KANNGIEßER, B., MALZER, W., MANTOUVALOU, I., SOKARAS, D. & KARYDAS, A.G. (2012). A deep view in cultural heritage – confocal micro X-ray spectroscopy for depth resolved elemental analysis. *Applied Physics A* **106**, 325–338.

LINDQVIST, J.E. & ÅKESSON, U. (2001). Image analysis applied to engineering geology, a literature review. *Bulletin of Engineering Geology and the Environment* **60**, 117–122.

MALOY, A.K. & TREIMAN, A.H. (2007). Evaluation of image classification routines for determining modal mineralogy of rocks from X-ray maps. *American Mineralogist* **92**, 1781–1788.

MALZER, W. & KANNGIEßER, B. (2005). A model for the confocal volume of 3D micro X-ray fluorescence spectrometer. *Spectrochimica Acta Part B* **60**, 1334–1341.

MANTOUVALOU, I., WOLFF, T., HAHN, O., RABIN, I., LÜHL, L., PAGELS, M., MALZER, W. & KANNGIESSER, B. (2011). 3D micro-XRF for Cultural Heritage objects: New analysis strategies for the investigation of the Dead Sea scrolls. *Analytical Chemistry* **83**, 6308–6315.

MARITAN, L., MAZZOLI, C., SASSI, R., SPERANZA, F., ZANCO, A. & ZANOVELLO, P. (2013). Trachyte from the Roman aqueducts of Padua and Este (north-east Italy): a provenance study based on petrography, chemistry and magnetic susceptibility. *European Journal of Mineralogy* **25**, 415–427.

MERA, M.F., RUBIO, M., PÉREZ, C.A., GALVÁN, V. & GERMANIER, A. (2015). SR μXRF and XRD study of the spatial distribution and mineralogical composition of Pb and Sb species in weathering crust of corroded bullets of hunting fields. *Microchemical Journal* **119**, 114–122.

MILANI, L., BECCALUVA, L. & COLTORTI, M. (1999). Petrogenesis and evolution of the Euganean Magmatic Complex, Veneto Region, North-East Italy. *European Journal of Mineralogy* **11**, 379–399.

OZTURK, C.A. & NASUF, E. (2013). Strength classification of rock material based on textural properties. *Tunnelling and Underground Space Technology* **37**, 45–54.

PREVIATO, C., BONETTO, J., MAZZOLI, C. & MARITAN, L. (2014). Aquileia e le cave delle regioni alto-adriatiche: il caso della trachite euganea. In *Arqueología de la construcción IV. Las canteras*

en el mundo antiguo: sistemas de explotación y procesos productivos, Bonetto, J., Camporeale, S. & Pizzo, A. (Eds.), pp. 149–166. Mérida: CSIC.

PŘIKRYL, R. (2006). Assessment of rock geomechanical quality by quantitative rock fabric coefficients: limitations and possible source of misinterpretations. *Engineering Geology* **87**, 149–162.

RENZULLI, A., ANTONELLI, F., SANTI, P., BUSDRAGHI, P. & LUNI, M. (1999). Provenance determination of lava flagstones from the Roman 'Via Consolare Flaminia' pavement (central Italy) using petrological investigations. *Archaeometry* **41** (2), 209–226.

RENZULLI, A., SANTI, P., NAPPI, G., LUNI, M. & VITALI, D. (2002a). Provenance and trade of volcanic rock millstones from Etruscan-Celtic and Roman archaeological sites in Central Italy. *European Journal of Mineralogy* **14**, 175–183.

RENZULLI, A., SANTI, P., SERRI, G. & LUNI, M. (2002b). The Euganean trachyte flagstones ("basoli") used by the Romans along the mid-Adriatic coast (Marche, central Italy): an archaeometric study. *Periodico di Mineralogia* **71**, 189–201.

RINDBY, A. & JANSSENS, K. (2002). Microbeam XRF. In *Handbook of X-Ray Spectrometry*, Van Grieken, R.E. & Markowicz, A.A. (Eds.), pp. 631–718. New York: Marcel Dekker.

SANTI, P. & RENZULLI, A. (2006). Italian volcanoes as landmarks for the spreading of trade networks during the Etruscan and Roman periods: the millstones and flagstones case study. *Acta Vulcanologica* **18** (1-2), 133–140.

STEIGER, M., CHAROLA, A.E. & STERFLINGER, K. (2014). Weathering and deterioration. In *Stone in architecture. Properties, durability*, 5th edn., Siegesmund, S. & Snethlage, R. (Eds.), pp. 225–316. Berlin: Springer.

TARQUINI, S. & ARMIENTI, P. (2003). Quick determination of crystal size distributions of rocks by means of a color scanner. *Image Analysis & Stereology* **22**, 27–34.

TARQUINI, S. & FAVALLI, M. (2010). A microscopic information system (MIS) for petrographic analysis. *Computer & Geosciences* **36**, 665–674.

VAGGELLI, G. & COSSIO, R. (2012). μ-XRF analysis of glasses: a non-destructive utility for cultural heritage applications. *Analyst* **137**, 662–667.

VAGGELLI, G., LOVERA, V., COSSIO, R. & MIRTI, P. (2013). Islamic glass weights from Egypt. A systematic study by non-destructive μ-XRF technique. *Journal of Non-Crystalline Solids* **363**, 96–102.

WHITNEY, D.L. & EVANS, B.W. (2010). Abbreviations for names of rock-forming minerals. *American Mineralogist* **95**, 185–187.

Figure captions

Fig. 1. Photomicrographs in cross-polarised light of samples MNS-01 (*left*), MRL-03 (*centre*) and OLV-01 (*right*), taken at same magnification (field size: 9.71 x 13.07 mm). Anomalous interference colours of crystals are due to section thickness of 45 μm.

Fig. 2. X-ray maps of most significant elements from one sample from Monte Merlo (field size: 5.30 x 4.14 cm).

Fig. 3. Classified maps of samples MNS-01 (*top*), MRL-03 (*centre*) and OLV-01 (*bottom*) (field size: 5.30 x 4.14 cm). Colours not shown in legend: occasional phases. Abbreviations as in Table 1.

Fig. 4. Score and loading plots from PCA on: (a) modal composition of all samples (variables as in Table 2, excluding P.I.), PC1, PC2 and PC3 covering 35%, 26% and 12% of total variance, respectively; (b) crystal-size data of feldspars of all samples (Feret diameter and area classes as in Table 3) and percentages (anorthoclase, plagioclase and sanidine, as in Table 2), with PC1, PC2 and PC3 covering 65%, 15% and 10% of total variance, respectively.

Fig. 5. Frequency histograms of crystal-size distribution of feldspars, based on areas larger than 1 mm^2 for each particle analysed, calculated for samples MNS-01 (*left*), MRL-03 (*centre*) and OLV-01 (*right*).

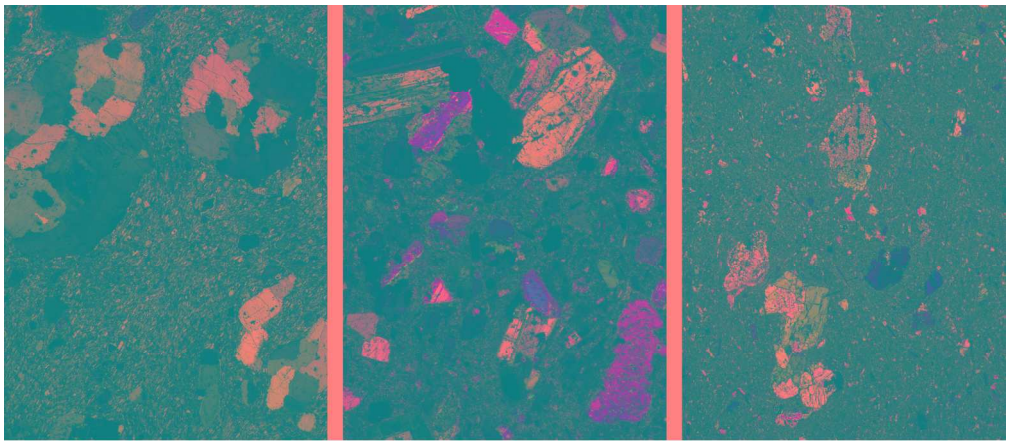

Fig. 1. Photomicrographs in cross-polarised light of samples MNS-01 (left), MRL-03 (centre) and OLV-01 (right), taken at same magnification (field size: 9.71 x 13.07 mm). Anomalous interference colours of crystals are due to section thickness of 45 µm.
82x35mm (600 x 600 DPI)

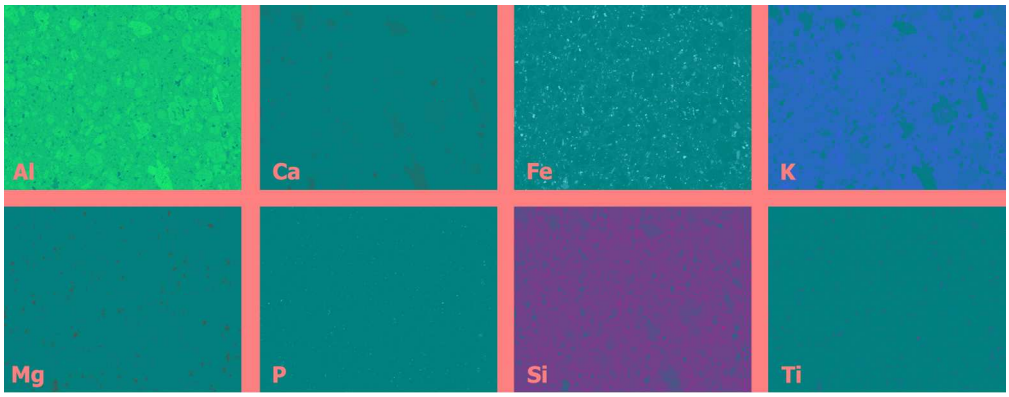

Fig. 2. X-ray maps of most significant elements from one sample from Monte Merlo (field size: 5.30 x 4.14 cm).
189x73mm (300 x 300 DPI)

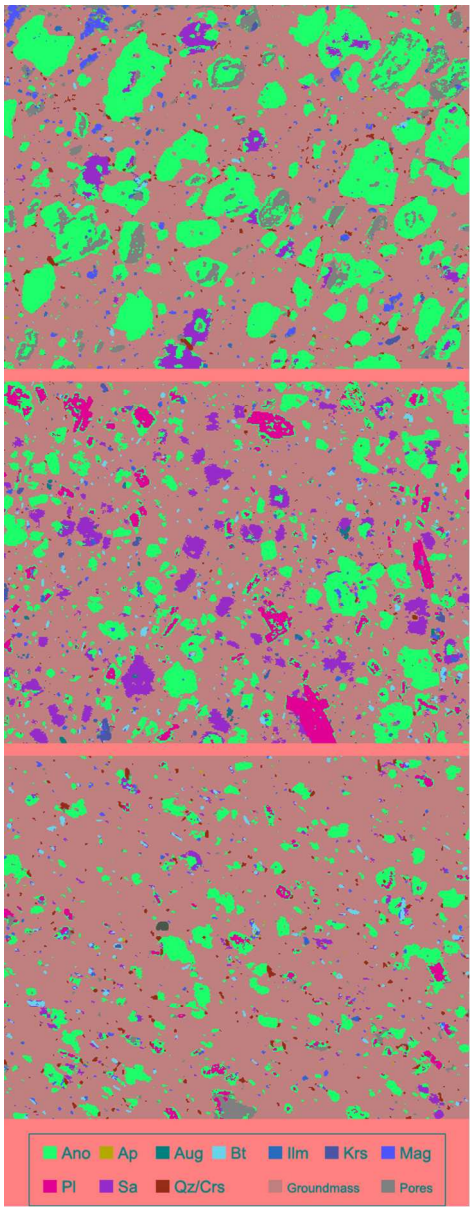

Fig. 3. Classified maps of samples MNS-01 (top), MRL-03 (centre) and OLV-01 (bottom) (field size: 5.30 x 4.14 cm). Colours not shown in legend: occasional phases. Abbreviations as in Table 1.
90x232mm (300 x 300 DPI)

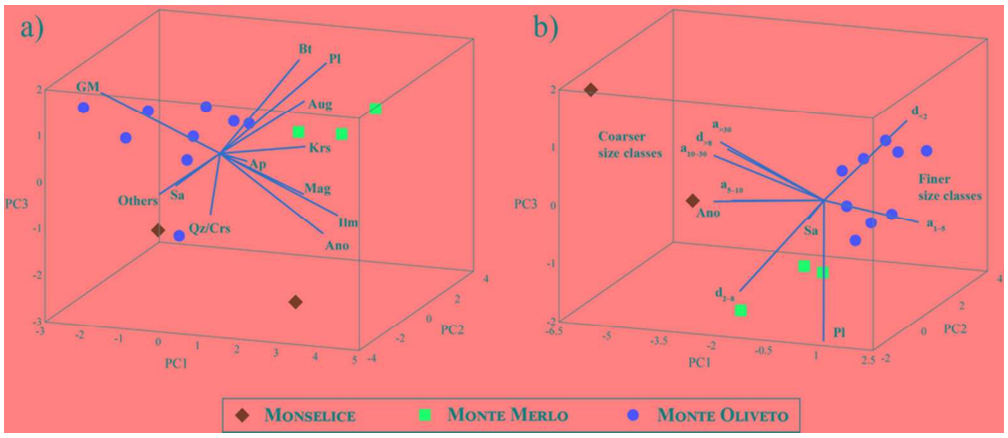

Fig. 4. Score and loading plots from PCA on: (a) modal composition of all samples (variables as in Table 2, excluding P.I.), PC1, PC2 and PC3 covering 35%, 26% and 12% of total variance, respectively; (b) crystal-size data of feldspars of all samples (Feret diameter and area classes as in Table 3) and percentages (anorthoclase, plagioclase and sanidine, as in Table 2), with PC1, PC2 and PC3 covering 65%, 15% and 10% of total variance, respectively.
81x34mm (300 x 300 DPI)

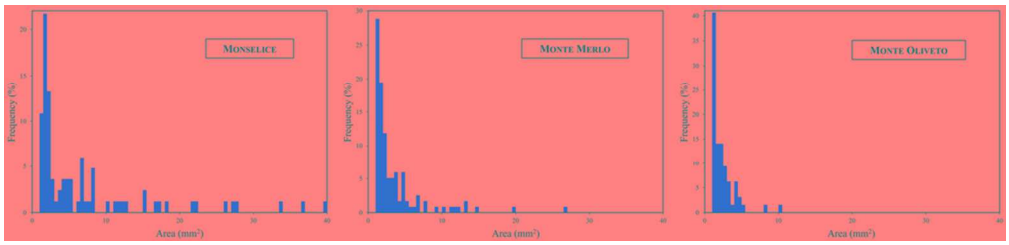

Frequency histograms of crystal-size distribution of feldspars, based on areas larger than 1 mm^2 for each particle analysed, calculated for samples MNS-01 (left), MRL-03 (centre) and OLV-01 (right).
44x10mm (600 x 600 DPI)

Table 1. Petrographic features of trachyte samples microscopically observed on thin section. Mineralogy reports mineral phases occurring in all samples from same quarry locality (phases in brackets: not always present). Abbreviations for minerals according to (Whitney and Evans, 2010): Ano = anorthoclase, Ap = apatite, Aug = augite, Bt = biotite, Crs = cristobalite, Ep = epidote, Ilm = ilmenite, Krs = kaersutite, Mag = magnetite, Pl = plagioclase, Qz = quartz, Sa = sanidine, Ttn = titanite, Zrn = zircon.

Quarry locality	Sample	Quarry	Mineralogy	Texture
Monselice	MNS-01 MNS-05	1	Ano, Sa, Bt, Krs, Mag, Ilm, Ap, Ttn	Holocrystalline and porphyric-glomeroporphyric, with hiatal grain size and microcrystalline, trachytic-pilotaxitic matrix.
Monte Merlo	MRL-02 MRL-03 MRL-05	2 3 4	Ano, Pl, Sa, Bt, Krs, Aug, Crs, Mag, Ilm, Ap, Zrn, (Qz)	Holocrystalline and porphyric-glomeroporphyric-cumuloporphyric, with seriate grain size and microcrystalline, felty matrix.
Monte Oliveto	OLV-01 OLV-02 OLV-03 OLV-04 OLV-05 OLV-07 OLV-08 OLV-11 OLV-12	5 6 7 8 9	Ano, Pl, Bt, Mag, Ilm, Ap, Ep, (Sa, Krs, Aug, Crs, Qz, Ttn)	Holocrystalline and porphyric-glomeroporphyric-cumuloporphyric, with hiatal grain size and cryptocrystalline, felty matrix. In some cases, groundmass is locally oriented, with a trachytic-pilotaxitic texture.

Table 2. Percentage of mineral phases constituting phenocrysts, percentage of groundmass (GM) and porphyritic index (P.I., corresponding to percentage area of all phenocrysts), calculated after particle analysis. ΣFsp = total feldspars. Abbreviations of minerals as in Table 1.

Quarry locality	Sample	Feldspars				Mafic minerals			Accessory minerals					GM	P.I.
		Ano	Sa	Pl	Σ Fsp	Bt	Aug	Krs	Qz/Crs	Ilm	Mag	Ap	Others		
Monselice	MNS-01	29.08	2.39	0.00	31.47	0.25	0.00	0.15	1.04	0.37	1.48	0.04	0.00	65.19	34.81
	MNS-05	12.76	9.43	0.00	22.19	0.33	0.00	0.14	0.00	0.31	0.74	0.04	0.10	76.15	23.85
Monte Merlo	MRL-02	14.52	0.65	6.88	22.05	2.15	0.04	0.03	1.29	0.40	1.82	0.23	0.00	71.99	28.01
	MRL-03	15.93	6.01	4.46	26.40	1.03	0.30	0.32	0.23	0.31	0.75	0.05	0.00	70.59	29.41
	MRL-05	19.42	0.96	5.47	25.85	1.11	0.69	0.37	0.33	0.38	1.10	0.06	0.00	70.09	29.91
Monte Oliveto	OLV-01	9.80	0.97	1.22	11.99	0.88	0.00	0.01	1.14	0.09	0.58	0.08	0.07	85.16	14.84
	OLV-02	10.20	0.63	2.85	13.68	0.69	0.00	0.02	0.28	0.15	1.60	0.14	0.00	83.45	16.55
	OLV-03	13.67	0.25	2.44	16.36	0.71	0.00	0.00	1.81	0.17	0.49	0.17	0.00	80.29	19.71
	OLV-04	11.36	0.29	3.19	14.84	1.62	0.00	0.04	1.77	0.20	0.51	0.07	0.00	80.94	19.06
	OLV-05	11.08	0.61	1.77	13.46	0.29	0.00	0.00	6.30	0.25	0.36	0.23	0.00	79.10	20.90
	OLV-07	15.96	0.72	5.22	21.94	1.64	0.00	0.06	2.42	0.16	0.27	0.17	0.00	73.38	26.62
	OLV-08	15.99	0.00	5.06	21.05	1.19	0.00	0.00	0.62	0.25	0.19	0.11	0.00	76.59	23.41
	OLV-11	10.32	1.28	1.50	13.10	0.94	0.00	0.05	0.69	0.09	0.25	0.11	0.00	84.77	15.23
	OLV-12	4.28	6.03	0.91	11.22	0.29	0.05	0.00	0.65	0.04	0.19	0.05	0.00	87.50	12.50

Table 3. Textural data of feldspars (anorthoclase, plagioclase and sanidine considered together) calculated after particle analysis. Feret diameter values subdivided into three classes (lower and upper limits of intermediate class at 2 and 8 mm); area values higher than 1 mm^2 subdivided into four classes (with limits at 5, 10 and 30 mm^2) and relative percentage frequency calculated. Perimeter (perim.), circularity (circ.) and aspect ratio (AR) values are averaged.

Quarry locality	Sample	Feret diameter (mm)					Area (mm^2)						Perim. (mm)	Circ.	AR
		Mean	Max	$d_{<2}$ (%)	d_{2-8} (%)	$d_{>8}$ (%)	Mean	Max	a_{1-5} (%)	a_{5-10} (%)	a_{10-30} (%)	$a_{>30}$ (%)			
Monselice	MNS-01	1.12	10.77	85.56	13.73	0.71	1.07	40.00	60.24	18.07	18.07	3.61	3.52	0.69	1.85
	MNS-05	1.40	10.37	82.67	16.67	0.67	1.28	41.15	67.86	23.81	5.95	2.38	4.72	0.62	1.90
Monte Merlo	MRL-02	0.85	6.15	90.63	9.37	0.00	0.41	15.37	85.05	12.15	2.80	0.00	2.38	0.71	1.94
	MRL-03	1.02	7.99	87.96	12.04	0.00	0.63	26.96	83.90	8.47	7.63	0.00	3.01	0.66	1.93
	MRL-05	1.31	9.69	84.72	15.15	0.13	0.83	34.94	80.34	13.68	5.13	0.85	3.87	0.62	2.02
Monte Oliveto	OLV-01	0.75	6.95	92.11	7.89	0.00	0.29	10.21	95.31	3.13	1.56	0.00	1.98	0.74	1.95
	OLV-02	0.86	4.13	90.32	9.68	0.00	0.39	7.63	97.67	2.33	0.00	0.00	2.32	0.75	1.85
	OLV-03	0.91	7.13	91.87	8.13	0.00	0.41	13.86	84.42	12.99	2.60	0.00	2.44	0.74	1.89
	OLV-04	0.80	7.46	93.56	6.44	0.00	0.37	13.20	86.36	10.61	3.03	0.00	2.13	0.73	1.90
	OLV-05	0.74	5.12	93.57	6.43	0.00	0.34	6.90	90.28	9.72	0.00	0.00	1.95	0.78	1.85
	OLV-07	0.80	8.53	92.88	7.04	0.08	0.38	13.28	88.78	9.18	2.04	0.00	2.14	0.78	1.84
	OLV-08	0.88	7.83	91.10	8.90	0.00	0.43	9.61	92.92	7.08	0.00	0.00	2.62	0.73	1.88
	OLV-11	1.04	4.88	88.04	11.96	0.00	0.56	7.22	93.83	6.17	0.00	0.00	2.91	0.72	1.89
	OLV-12	0.90	5.51	92.72	7.28	0.00	0.43	6.57	93.65	6.35	0.00	0.00	2.50	0.75	1.76